Effects of Compactor Footprints on the Response of Subgrade Soil

JEFF BUDIMAN AND JOHANES WIBOWO

The influence of compactor footprints on the constitutive response of clayey sand subgrade soil was investigated. Three footprint types—flat base, cylindrical protrusion, and pyramid frustum protrusion—were examined using triaxial tests and pavement model tests under dynamic loading. First, each block sample was prepared using the compactor of certain footprint. The triaxial specimens were trimmed from the block sample at different orientations to represent the rotation of the principal stress direction. The results show significant variations in the responses. Samples compacted by the compactor with pyramid frustum protrusion base showed the highest lateral stiffness, followed by samples compacted with cylindrical protrusion, and finally those compacted with the smooth footprint. However, samples compacted with the flat base showed the stiffest response in the vertical direction. The subgrades of the pavement models were each compacted to the same density using compactors with different footprints. A dynamic load of 448 kPa was applied on the pavement model through a plate. Linear voltage displacement transformers and photographic techniques measured the deformation of the soil elements within the subgrade. The results show that, although the subgrade of the models were of the same density, the monitored displacements of elements within each pavement system were significantly influenced by the footprint type used during compaction. Traces of the displaced points show a significant variation of the deflection curve at the interlayer, which reflects rutting.

The performance of a flexible pavement is influenced by many factors, such as the asphalt type, asphalt content, aggregate type, gradation, density, subgrade type, compaction method, temperature, climate, magnitude and frequency of loads, and other variables. The interaction of all these factors yields a composite behavior for a particular pavement structure that can become evident in the form of distress, such as cracking, rutting, and potholes.

Approximately 70 percent of the total surface deflection of the pavement occurs within the subbase and subgrade soil. Figure 1, which illustrates the major principal stress distribution within the pavement system under the wheel load shows that the magnitude and the orientation of the major principal stresses vary from element to element within the system. The direction of the major principal stress directly under the contact area is primarily vertical and gradually rotates to other directions as the stresses are distributed away from the loaded area. The change of the in situ principal stress magnitude and direction in the pavement system is repeated as the traffic continues to flow.

J. Budiman, Department of Civil Engineering, Illinois Institute of Technology, Chicago, Ill. 60616. J. Wibowo, University of Colorado, Boulder, Colo. 80302.

Previous studies (*1–4*) indicate that both sands and clays have the weakest constitutive response in the direction perpendicular to the past major principal stress direction. As shown in Figure 1, the vertical deflection of the pavement is not only controlled by the stiffness of the material in the vertical direction, but it is also significantly affected by its stiffness moduli in other directions. Therefore, if the lateral stiffness modulus of the material could be increased during construction, the vertical deflection would be reduced.

The selection of a compactor during construction is primarily based on the effectiveness of the energy transfer to a given volume of soil to achieve a specified density. It is known, however, that a compaction roller with smooth wheels compacts the soil by a kneading mechanism, whereas the sheepsfoot roller type uses a combination of shearing and kneading mechanisms (*5*). If the soil was compacted to the same density by two rollers of different footprint types, the soil fabrics produced would also be different, directly affecting their stiffness moduli. In the current design practice, the vertical stiffness modulus of the soil has been incorporated to a certain extent; however, the lateral stiffness modulus has been either excluded as a design criterion or assumed to be equal to the stiffness in the vertical direction (isotropic).

In this investigation, three different compactor footprint types were used to study their influences on the stress-strain behavior of compacted soil. The study was conducted in a series of dynamic triaxial tests. Models of pavement segment were also tested in the laboratory to examine their performance. The three types of compactor footprints used were flat (smooth), cylindrical protrusion base, and pyramid frustum protrusion base.

TEST MATERIAL AND SPECIMEN PREPARATION

The soil for this experiment consisted of 65 percent Ottawa sand No. 30, 5 percent silica silt, and 30 percent Kaolin clay representing the subgrade material. The soil had a liquid limit of 25 percent and plastic limit of 19 percent. The compaction test performed according to AASHTO Standard T-99 revealed the optimum moisture content (OMC) of 9.75 percent and the maximum dry density of 2.03 g/cm^3. Because most design specifications for construction require 95 percent relative compaction, the specimens were compacted to that standard. For the results reported herein, the dry density of the soil was 1.93 g/cm^3, and the moisture contents were 11.5 percent and 8.25 percent. The primary reason the sand was mixed with the cohesive soil was for specimen preparation purposes.

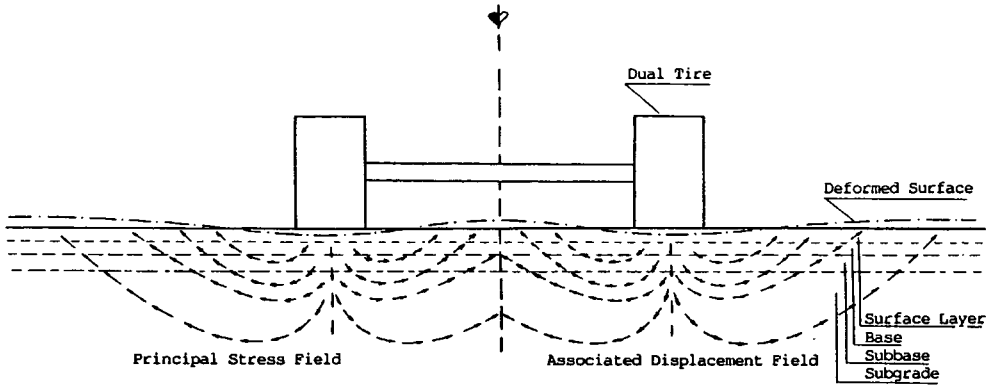

FIGURE 1 Approximate in situ principal stress field and associated displacement field.

The moisture and cohesion of the soil held the block specimen intact after compaction, enabling smaller specimens to be cut and trimmed from the large block specimen for further testing.

The soil was mixed with water to achieve the specified moisture content and then compacted in a large, stiff-walled mold of 20.32 × 30.48 × 25.4 cm to produce block samples. The block specimen was compacted in layers using the static undercompaction technique (*6*) to achieve a dry density of 1.93 g/cm^3. The compaction load was applied to the soil in the model through a rigid metal base plate in a universal loading machine, each plate representing a footprint type of the compactor. The three footprints represented were the flat smooth base, the sheepsfoot type with cylindrical protrusion, and the tampingfoot type with the pyramid frustum protrusion (Figure 2). The cylindrical protrusion was 12.7 mm in diameter and 25.4 mm high. The spacing of the protrusion was 3.5 times the diameter and was arranged in a triangular pattern. The pyramid frustum protrusion had the same height and volume as the cylindrical ones and was also arranged in the same pattern. The position of the projection on each layer was unchanged during compaction, that is, the location of each protrusion on the footprint of each succeeding layer was exactly above the previous one. The specimens for the triaxial testing were prepared from this large block sample.

Unlike the Directional Shear Cell (*1,7,8*), continuous stress rotation cannot be achieved in conventional triaxial testing. To simulate the rotation of the principal stress direction occurring within various soil elements in the subgrade, the triaxial specimens' axes were rotated. Three specimens were prepared from each block sample. Each specimen was cut and trimmed with its longitudinal axis rotated in a different orientation relative to the direction of compaction load: vertical ($\Psi = 0°$), inclined ($\Psi = 45°$), and horizontal ($\Psi = 90°$) (see Figure 3). These three specimens represented the three elements at different coordinates in the pavement system. The first specimen represented an element under the loaded area where the major principal stress direction is vertical. The second specimen represented an element where the major principal stress direction rotated to an inclined position. The third specimen represented an element where the major principal stress direction rotated to a horizontal position. The triaxial specimen was 71 mm in diameter and 152 mm high.

TRIAXIAL TEST RESULTS AND DISCUSSION

Two series of the dynamic triaxial tests were performed based on the specimen's moisture content, one test above OMC and the other below. Because the water content of the specimen was unchanged for each series of tests and the water content was insufficient to permit full saturation of the pores, there was no porewater pressure buildup during the test. The loading machine used in this experiment was the Material Testing System Closed-Loop Servo Hydraulic System Model 810.

The initial seating load was set at 34 kPa to simulate the overburden pressure. A confining pressure of 172 kPa was applied to the cell. This pressure represented approximate residual confining stress in the field. The maximum deviator stress was 275 kPa, representing the average wheel pressure within the subgrade soil. The cyclic haversine load with a frequency of 2 Hz was applied to the specimen. Because the effects of confining pressure and rate of loading in the cyclic triaxial tests have been studied by many investigators they will not be detailed here (*9–11*).

After all preliminary setting was completed, the software loaded the data and executed the test. During the test, the stress-strain data could be observed on a monitor screen or printed. Deformations during the test were recorded according to the following intervals; every cycle for the first 50 cycles, every 10th cycle for cycles 51 through 150, and every 50th cycle for cycles 151 through 10,000. The test was terminated after 10,000 cycles because the strains were relatively constant under the given load.

The results of the tests using samples with high moisture content are shown in Figures 4 through 8. Figure 4 shows the stress-strain response of samples compacted with the smooth flat base compactor. For the vertical specimen ($\Psi = 0°$), the total strain after 10,000 load cycles is about 0.56 percent, with a large percentage of the strain accumulated in the first few load cycles and little thereafter. This test result is also presented in the number of load cycles versus axial strain relationship as depicted in Figure 5. The same format is used to present other test results as well.

The maximum strain is defined here at maximum load, whereas the minimum strain is at the end of unloading; both curves show little increase in strain after the first few cycles.

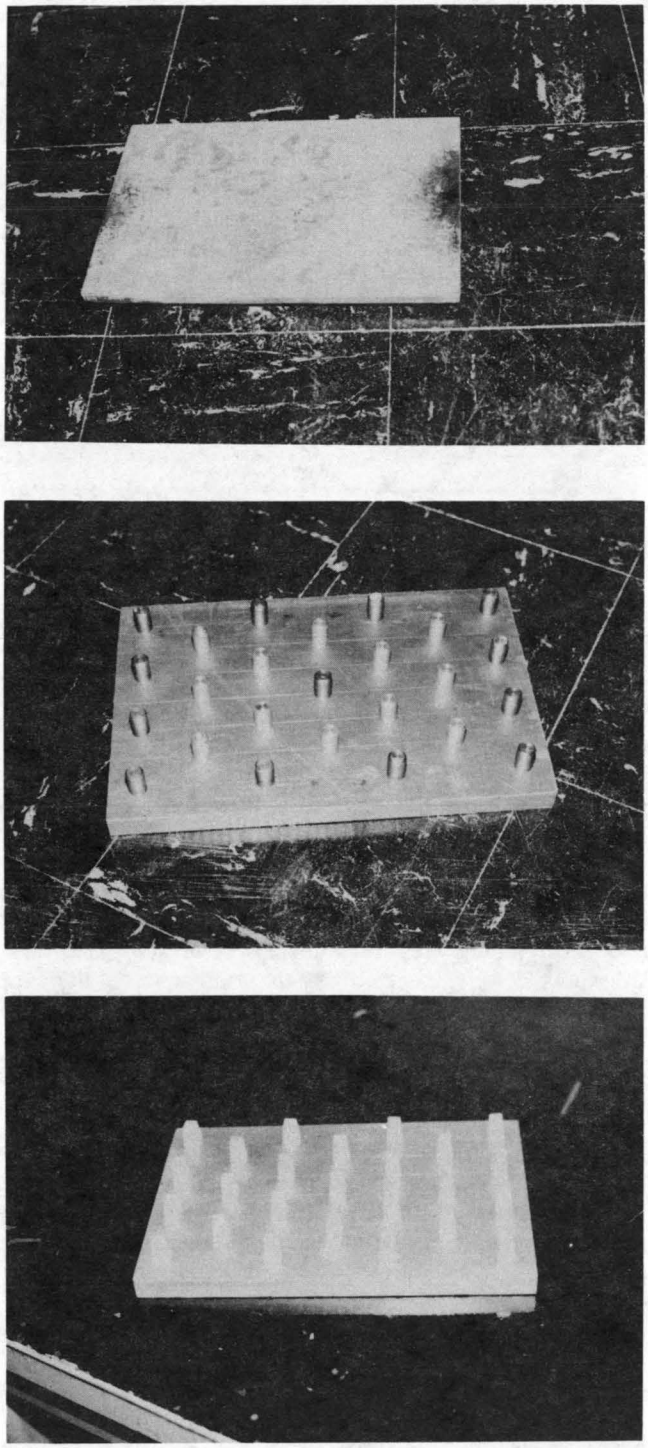

FIGURE 2 Compactor footprints: flat base (*top*), cylindrical protrusion (*middle*), pyramid frustum protrusion (*bottom*).

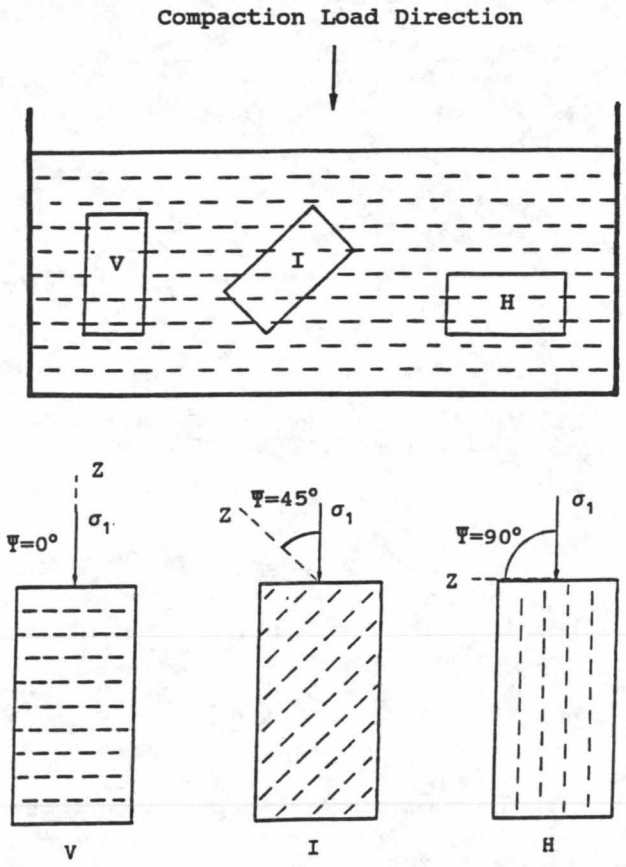

FIGURE 3 Triaxial specimens trimmed from block sample.

For the inclined specimen ($\Psi = 45°$), the response is similar to that observed in the vertical specimen; however, the magnitude of the strain is higher. For the same stress level and number of load applications, such as first cycle, the maximum strain in the vertical sample is 0.46 percent, whereas in the inclined sample the strain is 0.96 percent, or more than two magnitudes of the strain in the vertical sample. The permanent strain at the end of the test for the inclined sample is also significantly higher than the strain in the vertical sample.

The response of the horizontal sample ($\Psi = 90°$) under the same loading conditions shows a significant decrease in the stiffness modulus; here, the strain at the end of the test is 2.56 percent, or 460 percent higher than that of the vertical sample for the same loadings. In addition, unlike the response of the first and second samples, the total strain increases gradually with the number of load cycle.

The results of the tests for specimens compacted with the cylindrical protrusion compactor base are shown in Figure 6. The figure shows that the trends of the soil responses are similar to those observed in the sample compacted with the flat smooth base, that is, the largest total strain occurs in the horizontal sample followed by the inclined sample and vertical sample. Furthermore, a significant percentage of the total strain is accumulated during the earlier load cycles. However, the magnitude of the total strains for the horizontal and inclined samples are lower than the corresponding strains for specimens compacted with the flat base for the same loading condition. The total strains in the vertical samples are higher than the corresponding strains for samples compacted with the flat base.

The responses of specimens compacted with the pyramid frustum base compactor are shown in Figure 7. In general, the accumulation of the strain is similar to the previous cases, that is, the strains for the horizontal samples are always the largest compared to those of inclined and vertical samples,

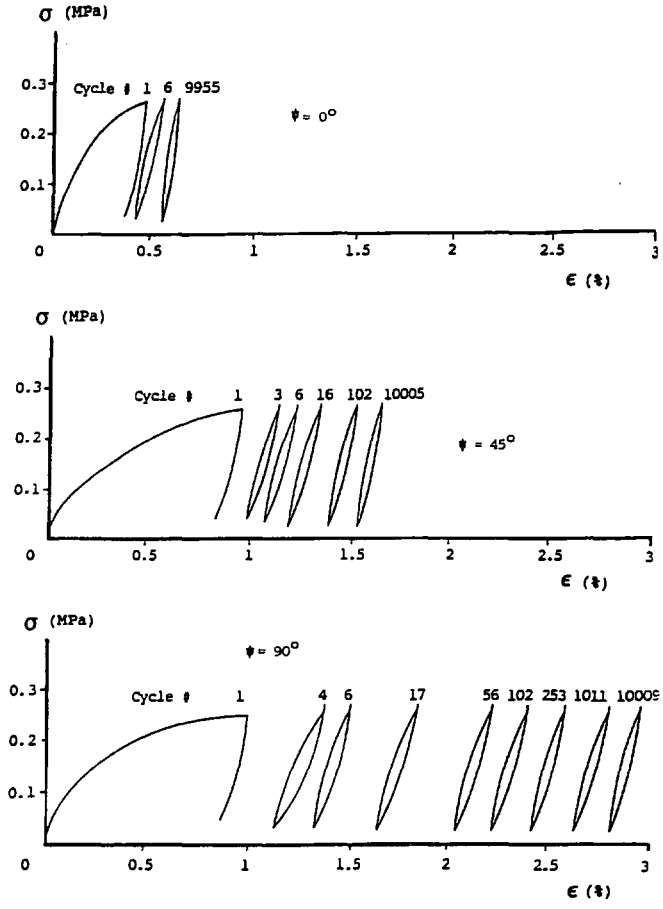

FIGURE 4 Stress-strain response of specimen compacted with flat base compactor, above OMC.

where the vertical samples produced the smallest strains. After 10,000 cycles of loading, the vertical sample produced about a 1.05 percent strain, whereas the horizontal sample produced a strain of 1.65 percent, or about 57 percent more strain than the vertical sample. The inclined sample produced a 1.45 percent strain, or about 38 percent more than the strain in vertical sample. Again, the stiffness modulus of the vertical sample is higher than that of the other two samples.

Figure 8 shows the response of the total strain with respect to the stress rotation angle relationship from all the tests above. A significant variation in strain occurred in the samples compacted with the flat base compactor, as indicated in Figure 8 by the steeper slope of the line drawn through the three points of the total strain. The slope of the curve for the samples compacted with pyramid protrusion base is the flattest among the three, showing less variation in the stiffness moduli of the material. An isotropic material would yield a perfect horizontal line. For the three vertical samples, the sample compacted with a flat base produced the lowest strain compared to those compacted with bases with cylinder or pyramid protrusions. However, for horizontal samples, the sample of flat base produced the largest strain. The strain from the three inclined samples shows the same tendency as for the horizontal samples, but to a lesser degree. The results show that samples compacted with a protruded base compactor result in less variation in the stiffness of the samples in various directions. This observation also indicates that the lateral stiffness is significantly increased and thus the degree of anisotropy is reduced. The protrusion of pyramid frustum type is more effective than that of cylinder type in increasing the horizontal stiffness of the soil. This shows the effect of the protrusion shape. It is believed that the effectiveness of the pyramid protrusion in compacting the soil is that when the soil is being compressed, the inclined walls of the pyramid

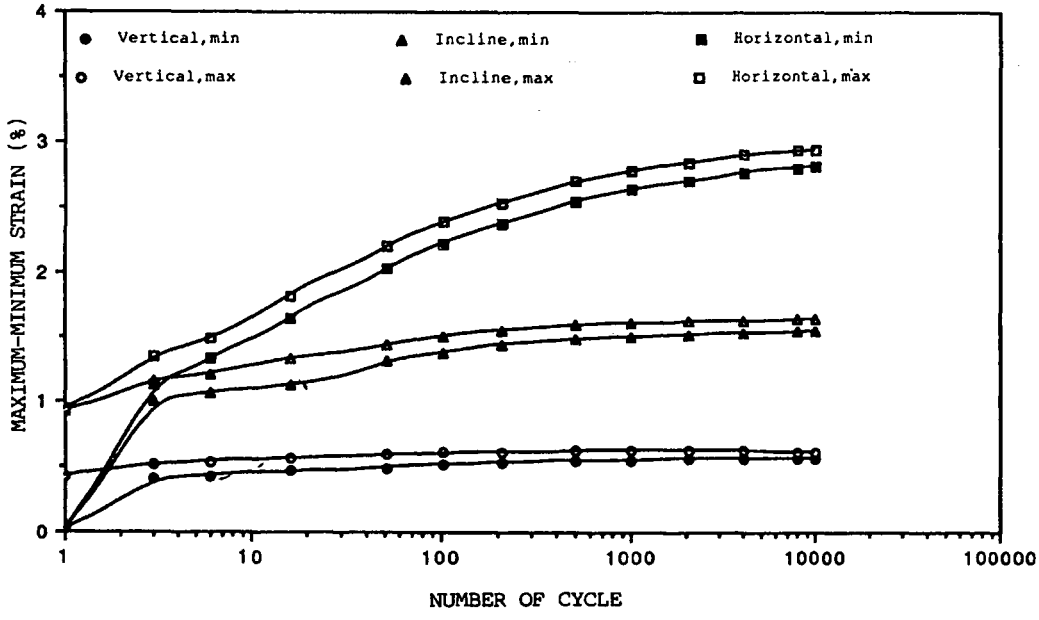

FIGURE 5 Strain versus load cycle response of specimens compacted with flat base, above OMC.

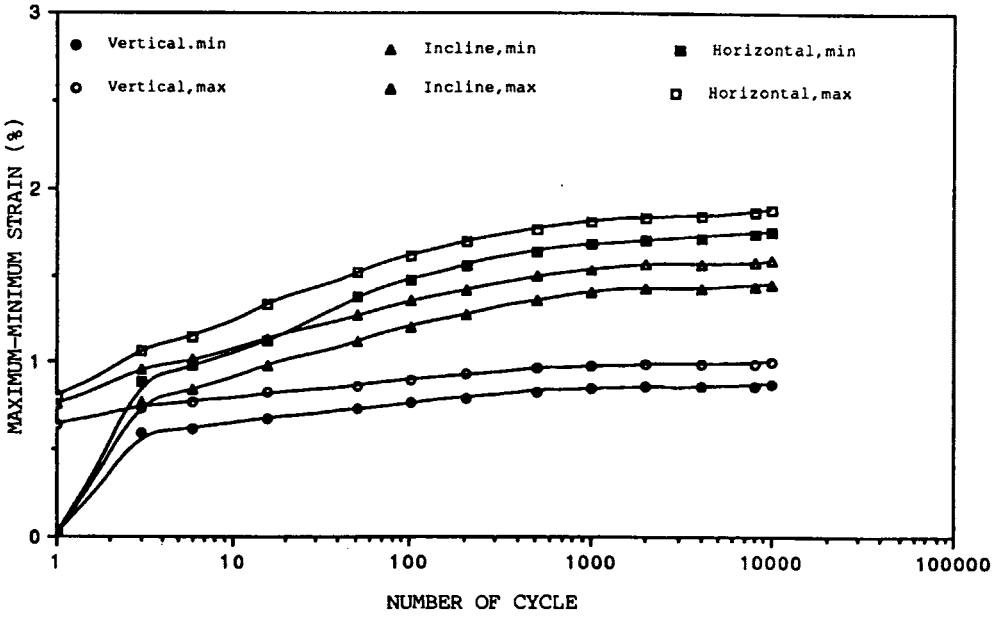

FIGURE 6 Strain versus load cycle response of specimens compacted with cylindrical protrusion base, above OMC.

also cause the soil to be displaced and thus compacted laterally as the protrusion penetrates into soil. At this stage, the lateral pressure in the soil generated by the inclined wall of the protrusion is higher than the lateral pressure generated with the soil when compacted with a flat base compactor or even with a cylinder type protrusion base.

In the second series of tests, the soil moisture content was reduced to 8.25 percent (below optimum). During compaction, significantly larger loads were required to compact this soil to achieve the same dry density than that of the soil with higher moisture content. These samples were much stiffer than the ones with higher water content. These phenomena are well known.

The response of specimens compacted by a flat footprint shows similar behavior as the ones compacted above OMC. The horizontal sample experienced the largest strain, followed by the inclined sample and the vertical sample, which experienced the smallest strain (Figure 9). The figure also shows that after 10,000 cycles of loading, the vertical sample produced about 0.32 percent strain, whereas the horizontal sam-

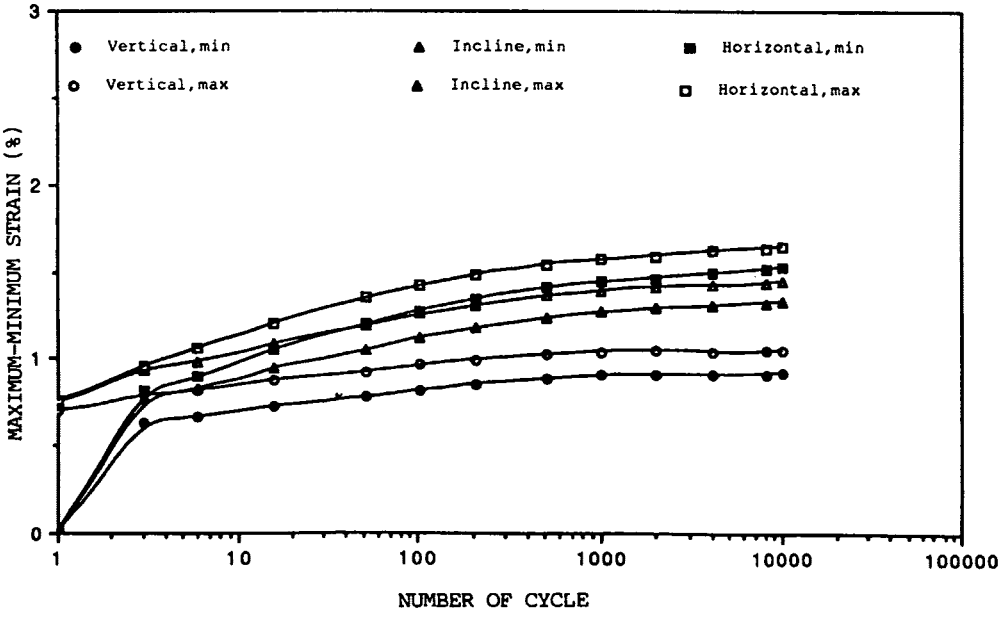

FIGURE 7 Strain versus load cycle response of specimens compacted with pyramid frustum base, above OMC.

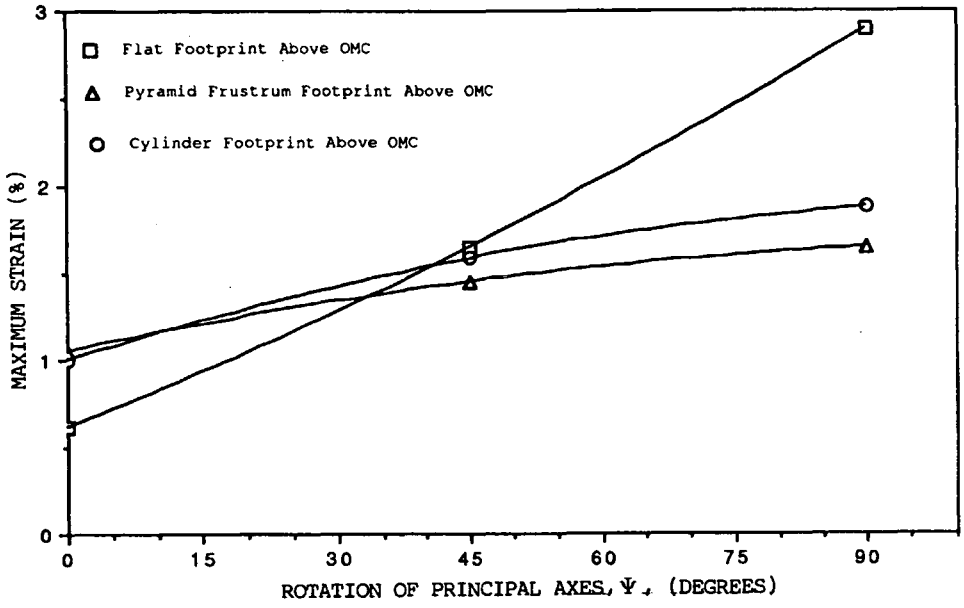

FIGURE 8 Maximum strain versus angle of principal stress direction response, above OMC.

ple produced a 0.62 percent strain, or about 94 percent higher than the strain for the vertical sample. The inclined sample produced a 0.48 percent strain, which is about 50 percent higher than the strain for vertical sample.

Figure 10 shows the results of the specimen compacted with a cylindrical protrusion footprint. The strain value of the horizontal sample is only slightly higher than that of the vertical sample. After 10,000 cycles of loading, the vertical sample produced about a 0.35 percent strain, while the horizontal sample produced a 0.37 percent strain or about 6 percent higher than the strain for vertical sample. The inclined sample produced a 0.45 percent strain, which is about 29 percent higher than the strain for the vertical sample.

Figure 11 shows the results on specimens compacted with the pyramid frustum base compactor. The trend depicted in Figure 11 is similar to that shown in Figure 10. After 10,000 cycles of loading, the vertical sample produced about a 0.34 percent strain, whereas the horizontal sample produced a strain of 0.37 percent, which is about 9 percent higher than the strain for the vertical sample. The inclined sample produced a 0.52 percent strain, which is about 53 percent higher than the strain for the vertical sample. The total strain and stress rotation

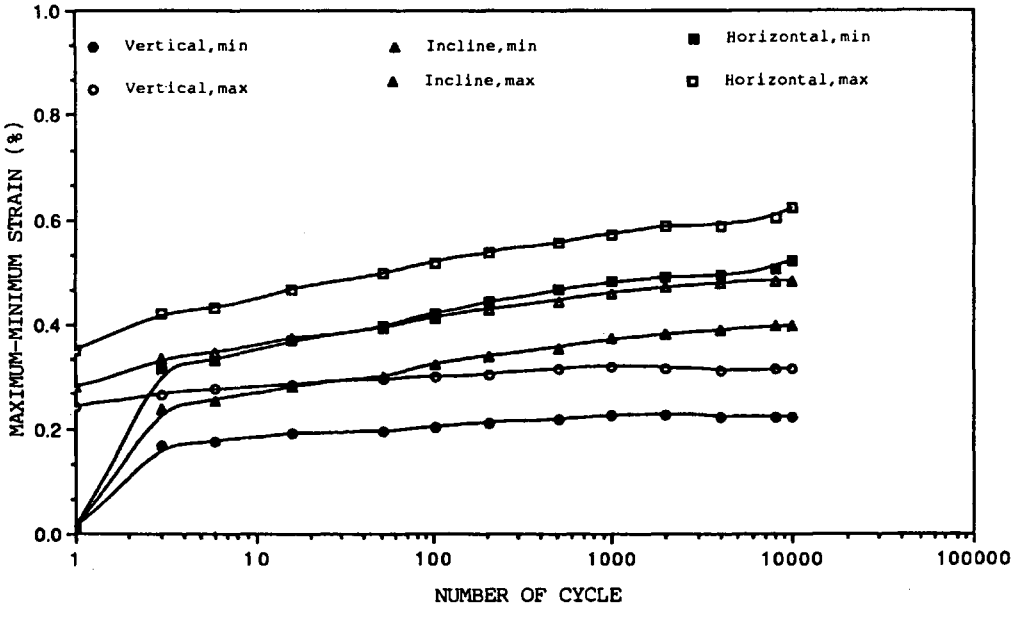

FIGURE 9 Strain versus load cycle response of specimens compacted with flat base, below OMC.

angle relationship depicted in Figure 12 shows that the protruded base resulted in stiffer samples; however, the shape of protrusion is insignificant.

As expected, the two series of tests revealed that the overall strains in the samples compacted at a lower water content are smaller than those compacted at a higher water content. Comparing the results in Figures 8 and 12 for samples of a flat base compactor, the ratio of strain in the horizontal sample to the vertical sample is about 4.7 for a sample with a high moisture content and only 1.1 for a sample with a low moisture content. Furthermore, the effects of moisture content on the anisotropy can also be observed through the difference of strain in vertical and horizontal samples. For samples compacted with a flat base, the strain difference for below OMC samples is 0.3 percent, which is significantly less than 2.3 percent, the value for the specimens with water content above OMC. Considering the difference of the strains, the degree of anisotropy of the specimens is smaller in the

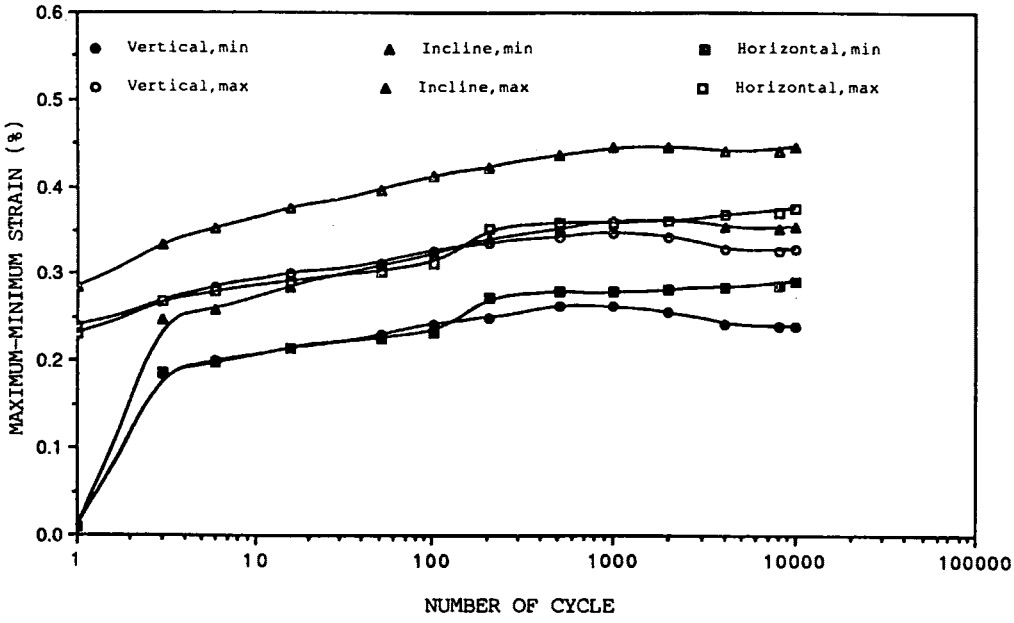

FIGURE 10 Strain versus load cycle response of specimens compacted with cylindrical protrusion base, below OMC.

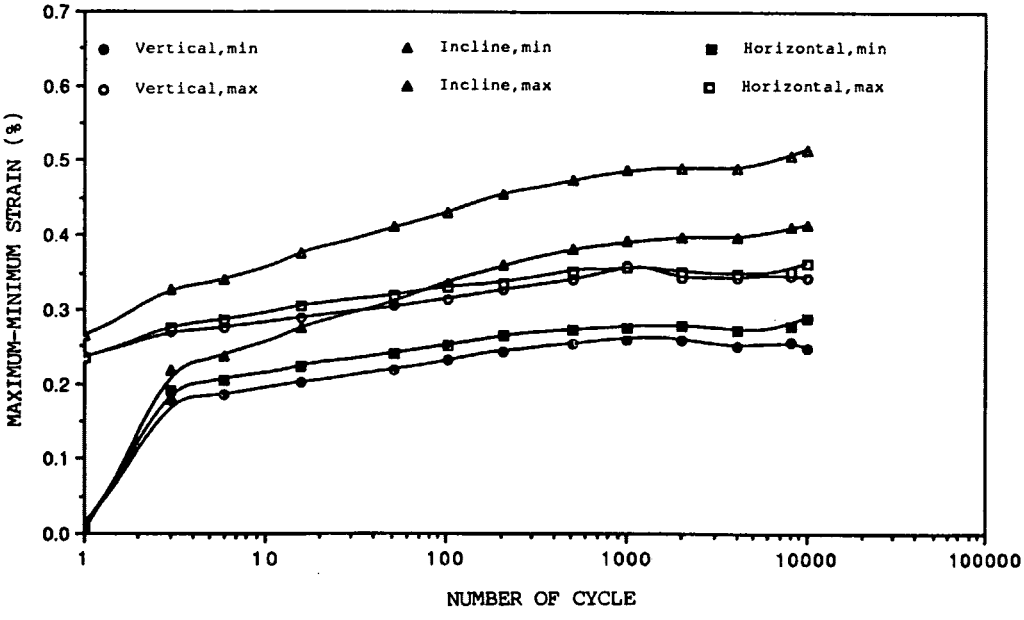

FIGURE 11 Strain versus load cycle response of specimens compacted with pyramid frustum base, below OMC.

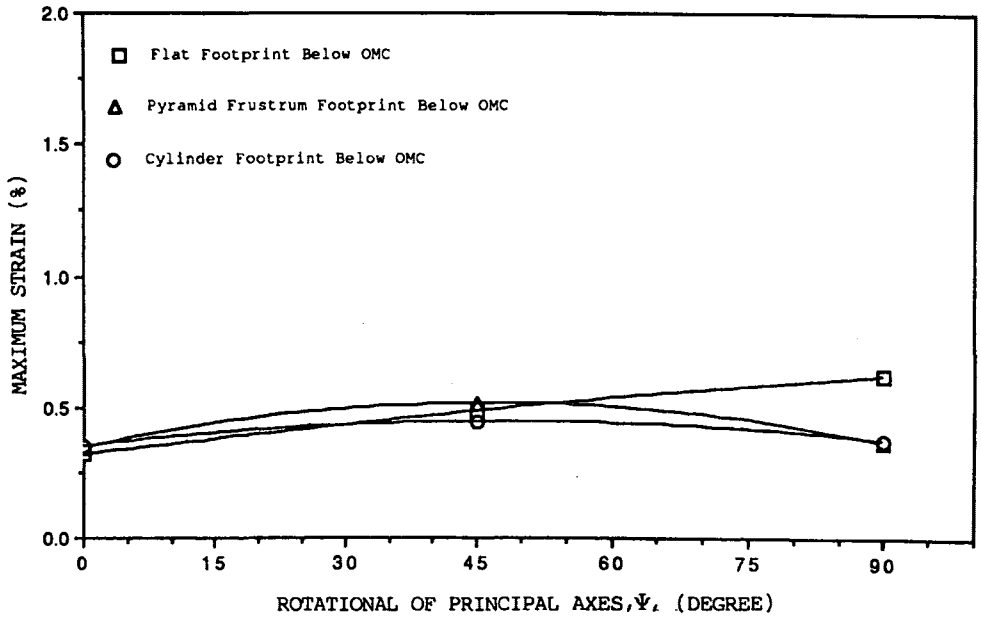

FIGURE 12 Maximum strain versus angle of principal stress direction response, below OMC.

specimens compacted below OMC than that in those compacted above OMC.

The results also show that, regardless of the type of footprint used, the specimens become anisotropic as a result of compaction. Consequently, they possess different characteristics in different directions with respect to the orientation of the compaction load (maximum pressure). In general, they are stiffer in the direction of maximum past pressure and softer or weaker in the direction perpendicular to the maximum past pressure, especially for samples compacted at a higher moisture content. The effects of the footprints on the constitutive response are also clearly depicted; the protrusion significantly increases the stiffness in the inclined and horizontal samples. The shape of the protrusion is more influential in samples that are above OMC than those below OMC.

MODEL TEST RESULTS AND DISCUSSION

Three model tests of each moisture content were performed in the laboratory to observe the influence of the types of compactor footprints on the deformation within the subgrade layer. These models represented a segment of the pavement system. Because the wheel load is symmetrical about the center of each lane of the roadway, only half of the section was necessary for modeling. Each model was compacted with the compactor having one of the three different types of footprints: the flat base, the cylindrical protrusion base, or the pyramid frustum protrusion base similar to those used for preparing triaxial specimens. The models were constructed in a Plexiglas box. The Plexiglas walls were reinforced with steel C-channels from the outside to provide rigid boundaries for plane strain conditions. The transparent walls allowed direct observation of the subgrade. The subgrade layer of 10.16 × 50.8 × 30.48 cm was compacted in 12 layers using the undercompaction method similar to that used in preparing the triaxial samples. For the asphalt layer of the model, cold ready-mixed asphalt was used and compacted to a density of 2 g/cm^3. Thin teflon sheets were placed between the walls and the soil to eliminate friction at the interface. To allow observation of the deformation within the subgrade, 12 slender steel rods of 2.5 mm in diameter were inserted into the subgrade model through holes drilled on one side of the wall. The monitoring rods were inserted in the subgrade at specified coordinates. During loading, linear voltage displacement transformers monitored and periodically recorded the horizontal and vertical displacements of the rods that were implanted in the subgrade. Deformation within the subgrade was also observed by photographing 88 pins in a grid pattern on the opposite side of the section. To implant these pins, the wall opposite to the side where the steel rods were inserted was temporarily removed, and 88 monitoring pins were inserted into the subgrade in a grid formation through the teflon sheet, exposing only the pinheads. The pinheads were periodically photographed to trace their movement.

The loading machine previously used for the dynamic triaxial tests was used in this experiment. The dynamic loads of passing vehicles were assumed as haversine loads. A square plate of 10.16 × 10.16 cm was mounted to the base of the loading ram. In turn, the dynamic contact pressure of 448 kPa was transferred to the center of the model through this plate.

The results of the three model tests with a high water content are presented in Figure 13. The deformations of five rods that were relatively far from the loaded area were too small to be analyzed. The analysis then focused on the results of the remaining seven rods: Rods 1–3, 5–7, and 9.

Rod 1 was located at the top of subgrade and below the center of the loaded area. For the model compacted with the flat base footprint, Rod 1 reached a vertical displacement of 4 mm after 500 load cycles. For models compacted with cylinder or pyramid frustum footprints, the same magnitude

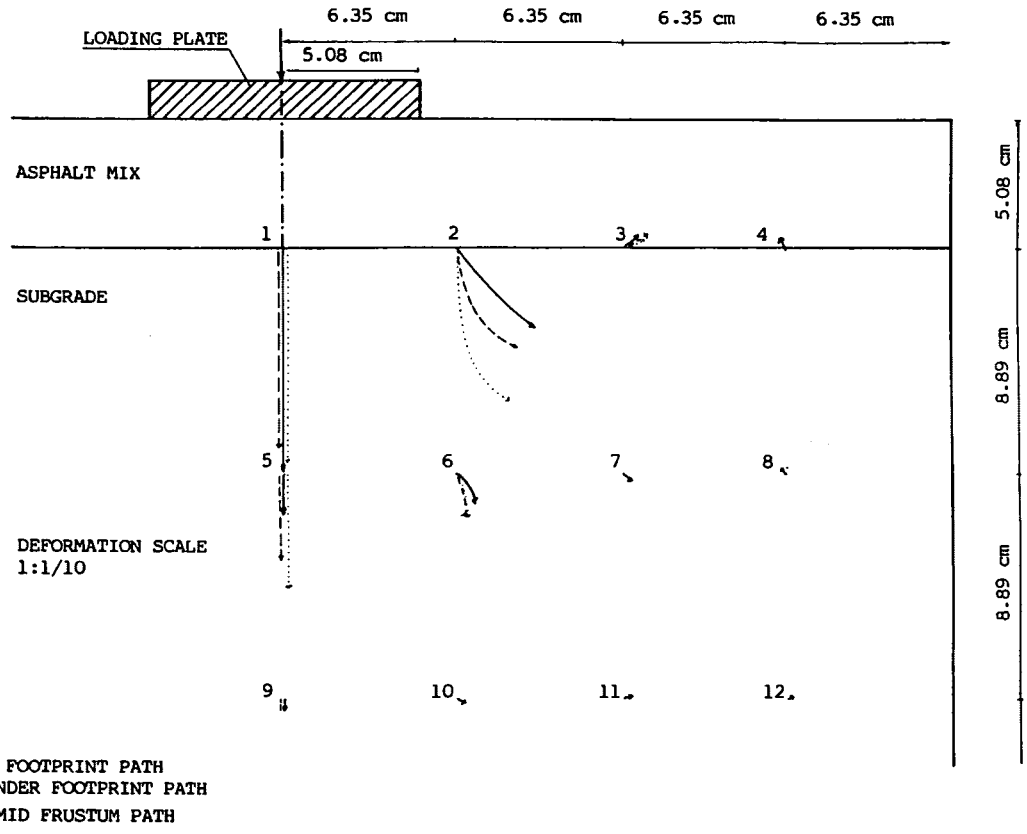

FIGURE 13 Displacement of rods within the pavement model, above OMC.

of displacement for Rod 1 was reached after only 25 load cycles. These observations show that the model compacted with the flat base compactor is stiffer in the vertical direction than the models compacted with a cylinder or pyramid frustum compactor.

After 10,000 load cycles, it was also observed that on Rods 2 and 6, the horizontal displacements were larger in the model compacted with the flat base compactor than in the models compacted with the cylinder or pyramid frustum compactor. To the contrary, the largest vertical displacement for these two rods occurred in the model compacted with the pyramid frustum compactor, followed by the displacement in the model compacted with the cylinder and flat base compactors, respectively.

Rods 3 and 4 moved upward from the loaded area; however, the magnitude was minuscule. Rods 5 and 9 on the model compacted with the flat base compactor deformed the least compared to the models compacted with cylinder or pyramid frustum base compactors. This shows that the model compacted with the flat base compactor is stiffer in the vertical direction than the other two models.

For the models compacted with a moisture content below optimum, after 10,000 load cycles, no measurable deformation of the rods was recorded. Subsequently, the load was increased to 620 kPa for each test to obtain measurable deformations. The results are presented in Figure 14. For Rods 1 and 5, the vertical displacements for the model compacted with the flat base compactor do not show significant difference in magnitude as opposed to the results from the models with a high moisture content. The response of Rod 5 showed less deformation in the sample compacted with the flat base footprint than the one with the cylindrical protrusion base. The displacement on Rods 2–4 and 6 indicates that the largest horizontal displacements occur in the model compacted with the flat base compactor. This observation is consistent with the results of the first series of tests, which show that the stiffness in the horizontal direction of the model compacted with the flat footprint is the lowest for both water contents.

Observation of the response of Rods 1–4, which were located at the interface between the asphalt layer and the subgrade soil, reveals that if a line were drawn connecting the arrow heads of the plot from each model test, the line would show that the worst rutting occurred in the model compacted with the flat footprint compactor. In the model with flat compactor, the vertical component of the displacement of Rods 3 and 4 were displaced relatively upward. In the other two models, these rods were not displaced upward. To control the density and uniformity of the specimens, the laboratory specimens were compacted using static compaction and did not simulate the conditions of field compaction.

CONCLUSIONS

The results of these model tests are consistent with the results of the dynamic triaxial tests. It is obvious that the subgrade layer is anisotropic and the stiffness modulus in the horizontal direction can be increased by using a compactor with a protrusion base. During construction, the type of compactor footprint used for compaction also significantly influences the load-deformation behavior of the soil. This was demonstrated

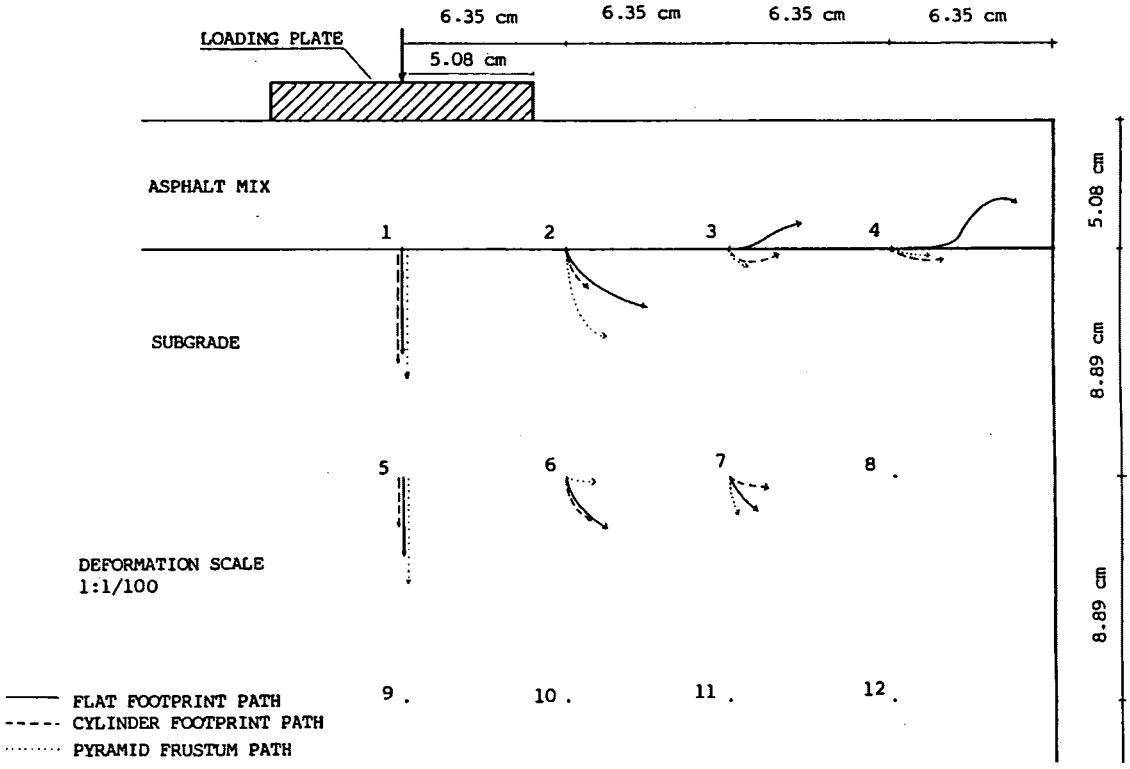

FIGURE 14 Displacement of rods within the pavement model, below OMC.

by the fact that all specimens in this study were compacted to the same dry density; however, they possessed different characteristics. This study also showed the importance of recognizing the material anisotropy because using the stiffness modulus in the vertical direction alone as a design criterion may result in a faulty prediction of the service life of the pavement. The study results suggest that compaction using a protruded wheel produces a pavement that better withstands rutting.

The goal of this study was to investigate the effects of the footprints on the material response under loading. This investigation used the static compaction method to avoid variation in the samples due to the compaction process. Because static compaction does not simulate a field compaction mechanism, further investigation on specimens compacted with rollers that have different types and sizes of footprints on various types of soils is highly recommended. Further study in this direction should reveal other critical information on how to improve the endurance of the subgrade material against permanent deformation.

ACKNOWLEDGMENTS

The authors greatly appreciate the financial support of the Engineering Foundation.

REFERENCES

1. S. Sture, J. S. Budiman, A. K. Ontuna, and H-Y. Ko. Directional Shear Cell Experiments on a Dry Cohesionless Soil. *Geotechnical Testing Journal*, ASTM, Vol. 10, No. 2, 1987.
2. M. Oda. Anisotropic Strength of Cohesionless Sands. *Journal of the Geotechnical Division*, ASCE, Vol. 107, GT9, 1981, pp. 1,219–1,231.
3. A. S. Saada and C. D. Ou. Stress-Strain Relations and Failure of Anisotropic Clays. *Journal SMF Division*, ASCE, Vol. 99, No. SM 12, 1973.
4. T. W. Lambe. The Engineering Behavior of Compacted Soil. *Journal SMFE*, Proc. Paper 1655, ASCE, Vol. 84, 1958.
5. R. D. Holtz and W. D. Kovacs. *An Introduction to Geotechnical Engineering*. Prentice-Hall, Englewood Cliffs, N.J., 1981.
6. R. S. Ladd. Preparing Test Specimen Using Undercompaction. *Geotechnical Testing Journal*, ASTM, Vol. 1, 1978, pp. 16–23.
7. J. R. F. Arthur, S. Bekenstein, J. T. Germain, and C. C. Ladd. Stress Path Tests with Controlled Principal Stress Directions. *Laboratory Shear Strength of Soil*, STP 740, ASTM, Philadelphia, Pa., 1980.
8. J. S. Budiman, S. Sture, and H-Y. Ko. Constitutive Behavior of Stress Induced Anisotropic Cohesive Soil. *Geotechnical Engineering Journal*, ASCE, Sept. 1992.
9. N. D. Pumphrey, Jr. and R. W. Lentz. Deformation Analysis of Florida Highway Subgrade Sand Subjected to Repeated Load Triaxial Tests. In *Transportation Research Record 1089*, TRB, National Research Council, Washington, D.C., 1986.
10. S. F. Brown and A. F. L. Hyde. The Significance of Cyclic Confining Stress in Repeated Load Triaxial Testing of Granular Materials. In *Transportation Research Record 537*, TRB, National Research Council, Washington, D.C., 1975.
11. H. B. Seed and C. K. Chan. Effect of Duration of Stress Application on Soil Deformation Under Repeated Loading. *Proc., Fifth International Conference on Soil Mechanics and Foundation Engineering*, Paris, 1961.

Publication of this paper sponsored by Committee on Transportation Earthworks.